Geomechanics and Engineering, *Vol. 40, No. 1 (2025) 33-45*
https://doi.org/10.12989/gae.2025.40.1.033

Study on the synergistic bearing characteristics and fracture evolution mechanisms of rock-like backfill specimens

Hu K. Wang[1a], Zhi G. Xia*[2,3], Hai L. Wang[4b], Bing Chen[5c], Jian Chen[6d] and Jin P. Cao[1e]

[1]*School of Civil Engineering, University of Science and Technology Liaoning, Anshan 114051, China*
[2]*School of Mining Engineering, University of Science and Technology Liaoning, Anshan 114051, China*
[3]*Engineering Research Center of Green Mining of Metal Mineral Resources Liaoning Province, Anshan 114051, China*
[4]*School of Civil Engineering and Architecture, Linyi University, Linyi 276000, China*
[5]*School of Civil Engineering, Shandong University, Jinan 250061, China*
[6]*School of Emergency Management and Safety Engineering, North China University of Science and Technology, Tangshan 063210, China*

(*Received August 20, 2024, Revised December 15, 2024, Accepted January 2, 2025*)

Abstract. The mechanical properties and fracture characteristics of goaf following tailings backfilling are crucial for exploiting deep resources. This study investigates the bearing characteristics and cracking behavior of hollow specimens and rock-backfill specimens with different diameters under uniaxial compression. The study examines the fracture evolution process driven by energy and analyzes the time-varying characteristics of acoustic emission (AE) parameters during loading. The results indicate that tailings backfilling enhances the peak strength and elastic modulus of the specimens, with the maximum increases being 38.87% and 66.41%, respectively. However, it does not alter the overall trend, which remains negatively correlated with the hollow diameter. As the diameter increases, the surface crack network phenomenon in hollow specimens gradually weakens. Rock debris transitions from small spalled and ejected pieces to larger spalled fragments. The crack propagation morphology of rock-backfill specimens exhibits a V-shaped distribution. The final failure mode of the specimens is a tensile-shear mixed failure, with shear failure being predominant. The internal backfill primarily exhibits shear slip failure. The input energy and elastic strain energy of the specimens are positively correlated with variations in mechanical parameters. Tailings backfilling reverses the trend of dissipation energy changes in the specimens compared to hollow specimens. At peak time, the dissipation energy of rock-backfill specimens with diameters of 25 mm and 30 mm is 2.4 and 2.09 times greater than that of the hollow specimens, respectively. The AE *b*-value of the rock-backfill specimens exhibits a secondary reduction phenomenon, and this phenomenon appears earlier as the diameter increases. The fluctuation in the RA value is substantial, indicating more severe stress release and crack propagation coalescence. As the diameter increases, the proportion of shear cracks initially increases and then decreases; however, the change range is more gradual in rock-backfill specimens, with a variation of about 4.25%. This study is of great significance for understanding the synergistic bearing behavior and fracture mechanisms of tailings backfill in the goaf.

Keywords: AE characteristics; energy evolution; fracture characteristics; synergistic bearing

1. Introduction

As surface resources continue to be depleted, the mining of solid resources, including minerals, is increasingly shifting to deeper levels (Hane *et al.* 2017, Yilmaz 2011). However, deep mining creates numerous underground cavities, severely disrupts the original stress environment, compromises the support of the overlying rock layers, and increases the risk of geological disasters such as surface collapse due to the gravity of the overlying rock layers and engineering disturbances (Palchik 2002, Choudhary and Kumar 2013). Consequently, ensuring the stability of underground goaf has become an urgent issue that needs to be addressed.

The use of tailings backfill can effectively restrain surrounding rock deformation in the goaf (Chiloane *et al*. 2024, Helinski *et al*. 2010, Sari *et al.* 2022), enhance underground goaf stability, increase mine economic benefits through resource recycling, and mitigate issues related to tailings stacking and environmental pollution (Ozcan *et al*. 2012, Kesimal *et al*. 2004, Siddique and Jang 2020, Kongar-Syuryun *et al*. 2021, Yilmaz *et al*. 2010). Consequently, scholars have conducted extensive research on this topic and achieved significant results (Li *et al*. 2021, Yan *et al*. 2022). Fall *et al*. (2005) explored the effect of tailings particle size on the microstructure and compressive strength of cemented paste backfill (CPB), and found that the proportion of fines tailings particles significantly affected its porosity and pore size distribution, which in turn affected its strength development. Kasap *et al*. (2022) analyzed the effect of tailings on the mechanical properties of CPB. The strength of the backfill increased with the increase of curing age, while the strength of the sulfide-rich tailings backfill decreased, and it was found that the pH value in the samples was related to the curing age. Kumar *et*

*Corresponding author, Professor
E-mail: xzgyy88@163.com

ISSN: 2005-307X (Print), 2092-6219 (Online)

al. (2016) showed that the flexural strength and flexural modulus of the cemented rock fill were linearly related to the cement content, and it was found that the splitting failure occurred first and then the shear failure occurred during the failure process. Fall *et al*. (2010) found that curing temperature is positively correlated with the uniaxial compressive strength of CPB, with the extent of influence depending on the CPB mixture composition and curing time. Xue *et al*. (2021) discussed the effects of fiber type and content, solid content and cement-sand ratio on crack resistance and post-peak toughness of cemented tailings backfill composites, and revealed the crack propagation mechanism and evolution law of fiber reinforced CTBC beam.

In fact, the fracture process of backfill is closely linked to the convergence and dissipation of energy (Hou *et al*. 2021, Kim *et al*. 2018, Ma *et al*. 2024). Additionally, as a non-destructive testing technique, AE can monitor the fracture evolution within the backfill in real time and assess its internal damage state (Shiotani 2006, Ullah *et al*. 2023). Zhou *et al*. (2023) analyzed the compressive strength and failure characteristics of CPB at different static rates, and discussed the effects of AE *b*-value and RA fractal dimension on crack evolution. Song *et al*. (2022) the damage process of prefabricated fracture CPB using energy conservation theory and examined the progressive damage pattern and cracking mechanism of the backfill through AE. Song *et al*. (2023) discussed the macroscopic mechanical properties and progressive damage evolution of the backfill by UCS test and AE monitoring. The destabilization precursor information of CPB and sulfate tailings-CPB (ST-CPB) was determined by using AE *b*-value and critical slowing down theory.

However, analyzing the bearing capacity of tailings backfill in isolation has certain limitations. In actual mining operations, complex interactions and synergistic effects exist between tailings backfill and surrounding rock (Aubertin *et al*. 2003, Golik and Efremenkov 2017). Many researchers have focused on the rock-backfill composite structure. Tan *et al*. (2020) investigated the mechanical properties and failure characteristics of cement-tailings backfill and rock core (CTB-RC) specimens, finding that the CTB-RC specimen showed a shear failure mode, and that the CTB could slow down the deformation speed of the inner rock core. Sharafisafa *et al*. (2019) found that the filling can significantly enhance the peak load of the specimens, and the filled specimens have a large fracture process zone before the peak load. Komurlu *et al*. (2016) explored the macroscopic fracture mode of sandstone-coal gangue-fly ash backfill (CGFB) specimens with different interface angles, and found that as the interface angle increased, the macroscopic fracture mode of sandstone-CGFB specimens shifted from splitting failure with local spalling to sliding failure along the interface.

Currently, extensive research has been conducted on the mechanical characteristics and failure modes of tailings backfill, yielding significant results. However, few studies have explored the interaction between tailings backfill and the actual goaf structure, particularly in scenarios that reflect real working conditions. Furthermore, research on the rock-backfill composite structures primarily addresses vertical (upper and lower) or horizontal (left and right) combinations. The synergistic bearing characteristics and fracture modes of rock-encased backfill remain insufficiently understood. This study investigates the bearing characteristics of hollow and rock-backfill specimens with varying structural attributes, analyzes their macroscopic fracture characteristics, and elucidates the internal damage evolution mechanisms based on energy conservation principles and AE parameters. The core objective is to reveal the mechanical behavior and fracture characteristics of goaf following tailings backfilling by integrating acoustic emission analysis and energy-based approaches, providing valuable insights for enhancing the stability of deep goaf and optimizing the design of mining structural parameters.

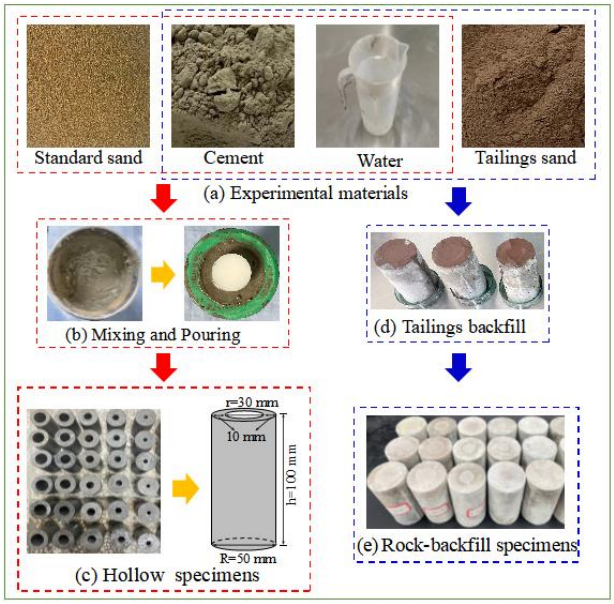

Fig. 1 Specimens preparation process

2. Experimental materials and methods

2.1 Specimen preparation

2.1.1 Hollow specimens

This study is based on the actual engineering background of Gongchangling Iron Mine in Anshan City, Liaoning Province, China, and carries out relevant design research on the basis of investigating the deep goaf rock layers of the iron mine. Through indoor rock mechanics experiments on on-site rocks, it is found that the range of rock strength is about 50 MPa~75 MPa, most of them are about 60 MPa. Therefore, this study takes the rock strength of the deep goaf of Gongchangling Iron Mine as a reference.

Hollow cylinder specimens were prepared using 3D printing technology to make the base model with a cylindrical cavity. Through continuous adjustment of the material ratios, the optimization experiment determined that

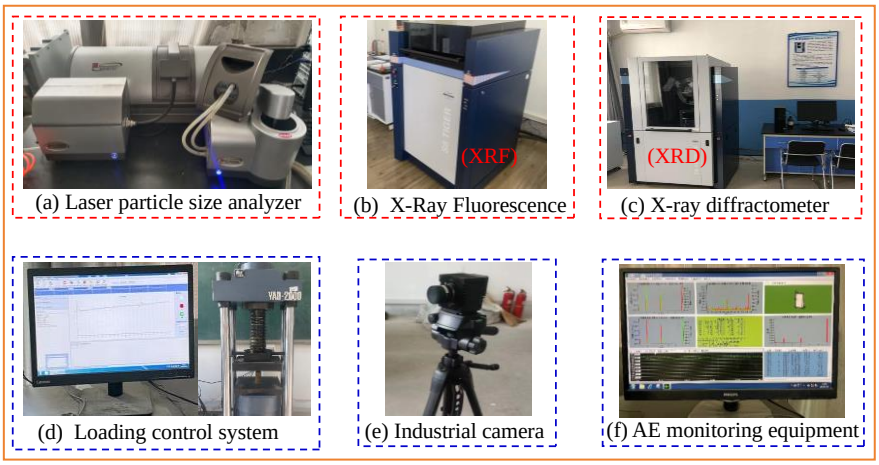

(a) Laser particle size analyzer (b) X-Ray Fluorescence (c) X-ray diffractometer

(d) Loading control system (e) Industrial camera (f) AE monitoring equipment

Fig. 2 Test equipment

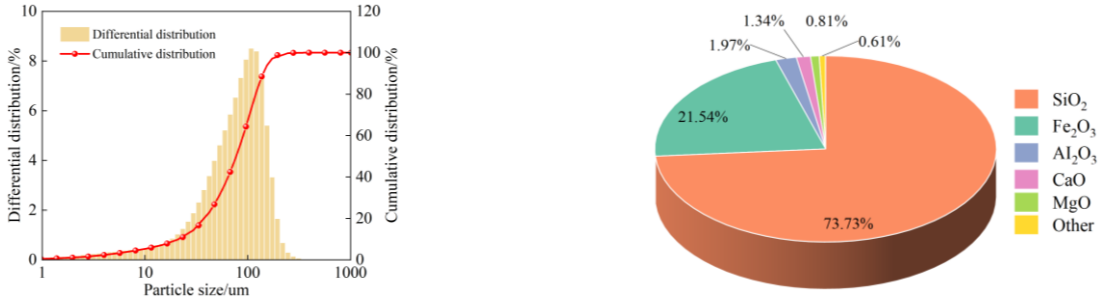

(a) Particle size distribution curve (b) Proportion of chemical composition

Fig. 3 Particle size distribution and composition ratio of tailings

a cement-to-standard sand ratio of 6:1 and a water-to-cement ratio of 0.35 could produce rock-like hollow cylindrical specimens. The cement used was P.O42.5 ordinary Portland cement, and the standard sand had a particle size ranging from 0.08 to 2 mm, as shown in Fig. 1(a). The cement, water, and standard sand were mixed according to the specified ratio and poured into a standard mold with a diameter of 50 mm and a height of 100 mm (the base model was fixed), as shown in Fig. 1(b). The mixture was then vibrated on a vibrating table until no bubbles appeared, after which the vibration was stopped, and the mixture was allowed to set initially. After an initial setting period of 7 hours, the base was removed, and the mold was demoulded after 24 hours. The specimens were then placed in a YH-40B standard constant temperature and humidity curing box for 28 days. The temperature was maintained at 20±5°C, and the relative humidity was set to 95±5 %. After curing, the upper and lower ends of each sample were polished flat and sealed with a preservative film. This study designed five different hollow diameters: 10 mm, 15 mm, 20 mm, 25 mm, and 30 mm, as shown in Fig. 1(c).

2.1.2 Rock-backfill specimens

Tailings were sourced from a mine in Liaoning Province. Rock-backfill specimens were prepared based on actual backfilling ratio parameters, using a cement-to-tailings ratio of 1:4 and a slurry mass concentration of 75% (Fu *et al*. 2020). The uniformly mixed slurry was slowly poured into the hollow sections of the cylindrical specimens. The slurry was then gently tapped to ensure it settled and filled the cavity, continuing until the slurry was level with the upper end of the specimens, as shown in Fig. 1(d). After the initial setting, the specimens were placed in a curing box for 28 days. The rock-backfill specimens after curing are shown in Fig. 1(e). Additionally, the hollow and rock-backfill specimens are labeled based on the hollow diameter. For instance, hollow specimens with a 10 mm diameter and rock-backfill specimens are designated as R-10 and RB-10, respectively.

2.2 Experimental equipment

2.2.1 Analytical equipment

The particle size of the dried tailings was analyzed using a Bettersize 2600 laser particle size analyzer. Component content analysis was performed using X-ray fluorescence (XRF) and X-ray diffraction (XRD), as shown in Figs. 2(a)-2(c). The median particle size (D50) of the tailings is 77.31 μm, with a coefficient of nonuniformity (Cu) of 5.16 and a coefficient of curvature (Cc) of 1.40, indicating good tailings gradation. The main chemical compositions of the tailings are SiO_2 and Fe_2O_3, accounting for approximately 95.27% of the total mass, classifying them as high-silica tailings, as shown in Fig. 3.

Table 1 Basic mechanical parameters of rock-like specimens and tailings backfill specimens

Material	Peak strength (MPa)	Elastic modulus (GPa)	Tensile strength (MPa)	Peak strain (10^{-3})
Rock-like specimens	58.78	10.82	6.14	8.79
Tailings backfill specimens	6.68	1.40	0.59	8.63

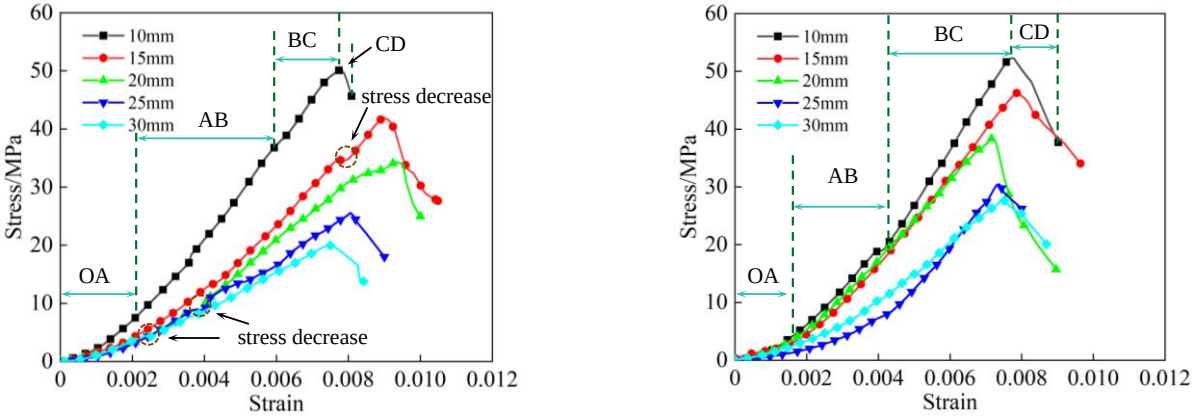

(a) Hollow specimens (b) Rock-backfill specimens

Fig. 4 Stress-strain curves of hollow specimens and rock-backfill specimens

2.2.2 Test equipment

The uniaxial compression tests were performed using a YAW-2000 kN micro-computer-controlled electro-hydraulic servo pressure testing machine, with a displacement rate of 0.2 mm/min. Use fine sandpaper to polish the ends of the specimen to minimize the end effect. An industrial camera was used concurrently to record the fracture process of the specimens. It has a resolution of 1936×1464 pixels and a frame rate of 408 frames per second. The AE monitoring system had a sampling frequency of 1 MHz and an acquisition threshold set to 40 dB. Two sets of four RS-2A integrated preamplifier sensors were arranged 20 mm from the upper and lower end faces of the sample and secured with rubber bands. The experimental equipment is shown in Figs. 2(d)-2(f). The basic mechanical properties of rock-like and tailings backfill specimens are summarized in Table 1.

3. Experimental results

3.1 Mechanical parameter change characteristics

Fig. 4 presents the stress-strain curves for hollow and rock-backfill specimens of varying diameters. As illustrated in the figure, the stress-strain curves of specimens with different diameter regardless of whether backfilling is performed have undergone four stages: compaction (OA), elastic deformation (AB), plastic deformation (BC), and post-peak failure (CD). For example, in the R-10 specimen during the OA stage, microcracks are gradually compressed and closed under load, causing a slow increase in the stress-strain curve. As loading continues into the AB stage, an approximately linear relationship between stress and strain is observed, with gradual internal damage. During the BC stage, internal stress redistribution leads to pronounced plastic deformation, reflected in the convex growth of the stress-strain curve. It is noteworthy that the plastic deformation stage in the rock-backfill specimen is not pronounced. This is attributed to the tailings filling the hollow inside the specimen, which improves the uniformity and continuity of its overall structure. Consequently, the stress distribution around the hollow becomes more uniform, leading to a more stable fracture of the specimen. In the CD stage, microcracks extend and coalesce into macroscopic cracks, ultimately causing instability and failure of the specimen.

Fig. 4(a) reveals differences in the stress-strain curves attributed to variations in hollow diameters. Stress fluctuations are observed in the R-15 to R-30 specimens, with strain values at the fluctuation points being 0.0079, 0.00421, 0.00391, and 0.00251, respectively. Specifically, as the hollow diameter increases, the strain at the stress fluctuation point decreases progressively. This phenomenon arises from the larger hollow diameter and reduced effective bearing section, which heightens local instability sensitivity and accelerates the onset of stress drop. Fig. 4(b) shows that the stress drop phenomenon is eliminated following tailings backfilling. Furthermore, the stress-strain curves for the RB-10, RB-15, and RB-20 specimens are closely clustered.

This indicates that tailings backfill effectively transfers and disperses external loads, allowing specimens to uniformly withstand external forces during loading. A comparison of the stress-strain curves for RB-20 and RB-25 reveals that the backfilling effect is significantly influenced by the hollow diameter size effect.

Fig. 5 illustrates the variation in peak stress and elastic modulus of the specimens. As shown in the figure, both the peak stress and elastic modulus of hollow specimens

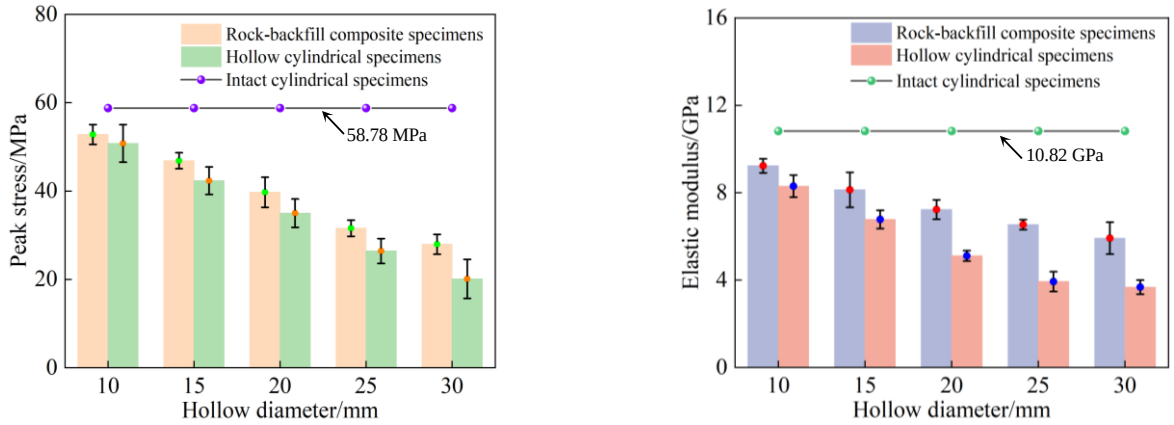

(a) Peak stress (b) Elastic modulus

Fig. 5 Average peak stress and elastic modulus of hollow specimens and rock-backfill specimens

(a) Standard rock-like specimen (b) Standard tailings backfill specimen

Fig. 6 Macroscopic failure mode of intact specimens

decrease as the hollow diameter increases. This indicates that a larger hollow diameter results in a smaller effective bearing area. With the same load, increased internal stress leads to greater susceptibility to deformation and failure.

The peak stress and elastic modulus for the R-30 specimen are approximately 20.12 MPa and 3.68 GPa, respectively. Compared to the intact specimen, these values are reduced by 65.77% and 65.99%, respectively, representing the highest reductions. Although the peak stress and elastic modulus of hollow specimens improve to some extent after tailings backfilling, the overall trend remains unchanged. Relative to the R-30 specimen, the RB-30 specimen exhibits the greatest improvement in peak stress, approximately 38.87%. For the elastic modulus, the RB-25 specimen shows the most significant improvement, approximately 66.41%.

3.2 Macroscopic failure mode

Fig. 6 depicts the final failure modes of both intact rock-like specimens and tailings backfill specimens. In the figure, the red circle denotes surface spalling, the blue arrow indicates shear cracks, and the yellow arrow represents tensile cracks. As shown in Fig. 6(a), the surface of the rock-like specimen primarily exhibits multiple tensile cracks, with secondary shear cracks developing during downward expansion. The predominant failure mode is a tensile-shear mixed failure. Additionally, there is minimal rock debris on the specimen's surface. The upper portion of the tailings backfill specimen exhibits significant damage, characterized by the extension of two tensile cracks and the absence of debris spalling. The low strength and elastic modulus of the tailings backfill specimen lead to particle interaction and rearrangement under compressive stress, causing local expansion and resulting in serrated dilatancy cracks, as depicted in Fig. 6(b).

Fig. 7 illustrates the final failure modes of hollow specimens, rock-backfill specimens, and specimens with internal backfills. Fig. 7(a) reveals a pronounced shear fracture zone on the surfaces of the R-10 and R-15 specimens, with significant rock debris and multiple secondary tensile cracks. For the R-20 specimen, as the tensile crack extends downward, its propagation direction changes twice. The crack type transitions from tensile to shear, with an increased crack width. The crack edges on the surfaces of the R-25 and R-30 specimens are relatively smooth, with a reduced broken area. The failure mode of hollow specimens is primarily characterized by tensile-shear mixed failure. As the hollow diameter increases, the crack propagation path becomes constrained. The network of interconnected cracks on the specimen's surface becomes progressively less pronounced. Rock debris transitions from small spalled and ejected pieces to larger spalled fragments. The cracking mode of the specimens becomes increasingly simplified.

Fig. 7(b) depicts the final failure mode of the rock-

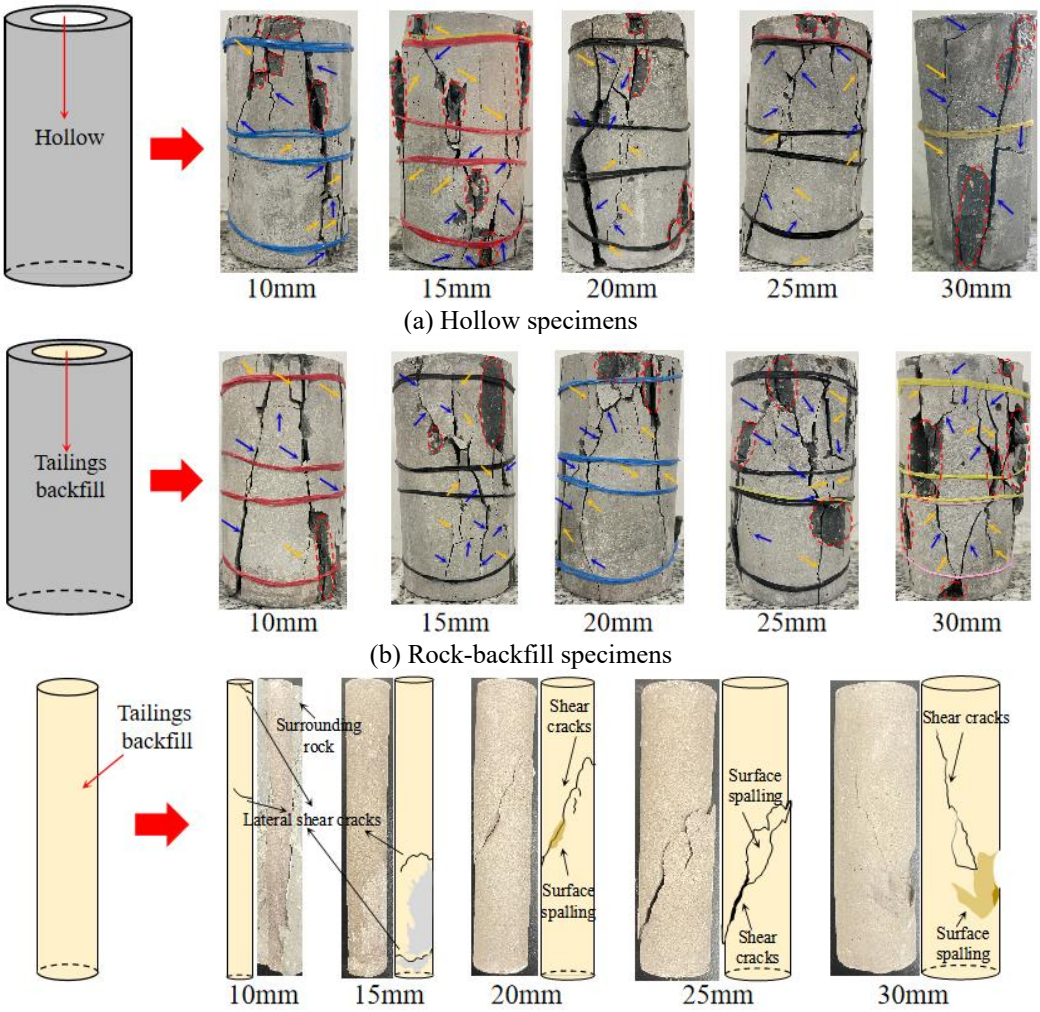

Fig.7 Final failure modes of hollow specimens, rock-backfill specimens and internal backfills

backfill specimens. The figure reveals that the crack propagation morphology of the specimens is similar, exhibiting a V-shaped distribution with additional crack branches. With increasing backfill diameter, the failure mode of the specimens becomes more complex. A significant fracture develops in the center of the RB-30 specimen, which is subsequently filled and densified by misplaced rock mass, contrary to the failure trend observed in hollow specimens. This is due to the fact that tailings backfilling enhances the overall bearing capacity of the specimens, leading to more severe damage at higher stress levels. Notably, the tailings backfill does not alter the failure mode, which remains a tensile-shear mixed failure.

Fig. 7(c) illustrates the final failure mode of the internal backfill. The figure shows that the failure characteristics of the backfill are clearly influenced by the backfill diameter. For backfill diameters of 10 mm and 15 mm, transverse shear cracks are primarily concentrated at both ends and the center, with minimal overall damage. For backfill diameters of 20 mm, 25 mm, and 30 mm, a macroscopic shear crack develops on the surface, accompanied by the formation and coalescence of two secondary shear cracks. The overall failure mode is shear slip, accompanied by debris spalling.

In comparison with Fig. 6(b), tensile cracks in the backfill are absent, and the expansion deformation is less pronounced. This is primarily due to the external constraining force from the surrounding rock, which reduces tensile stress within the backfill and limits its deformation, as depicted in Fig. 8.

3.3 Energy evolution law

The accumulation and release of energy during rock deformation and failure are dynamic and complex processes. Understanding the fracture behavior of rocks can be enhanced by investigating their energy evolution mechanisms. It is assumed that no heat exchange occurs between the rock and its surroundings during uniaxial compression. According to the first law of thermodynamics, the following can be derived (Song *et al*. 2022)

$$U = U_e + U_d \tag{1}$$

Where:U denotes the energy input from the external environment, U_e represents the elastic energy stored in the rocks, and U_d indicates the energy dissipated by the rocks.

(a) Standard tailings backfill specimen (b) Backfill in rock-backfill specimens

Fig. 8 Mechanical diagram under uniaxial compression test

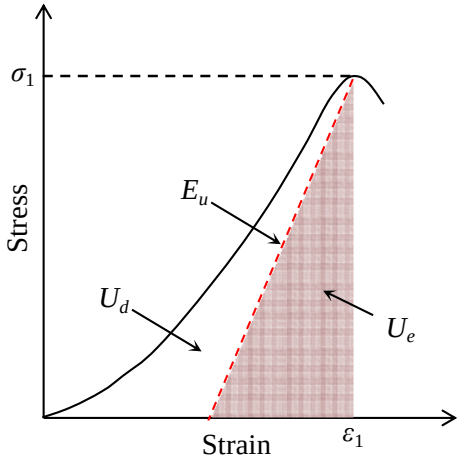

Fig. 9 Calculation principle diagram of elastic energy U_e and dissipation energy U_d under uniaxial compression

Fig. 9 illustrates the relationship between the energy components during uniaxial compression. The shaded area represents U_e, the unshaded area represents U_d , and the red dotted line indicates E_u, the unloading modulus. For calculating the elastic strain energy, the initial elastic modulus E_0 is used instead of the unloading elastic modulus E_u (Hou *et al*. 2021). Consequently, the formulas for calculating each type of energy are as follows

$$U = \int_0^{\varepsilon_1} \sigma_1 \mathrm{d}\varepsilon_1 \tag{2}$$

$$U_e = \frac{\sigma_1 \varepsilon^e}{2} = \frac{\sigma_1^2}{2E_u} \approx \frac{\sigma_1^2}{2E_0} \tag{3}$$

Fig. 10 illustrates the evolution of input energy, elastic strain energy and dissipation energy with strain. The figure reveals that the energy evolution patterns for hollow specimens and rock-backfill specimens are generally similar. Initially, during the loading phase, the specimens are in the compaction stage. At this point, the input energy, elastic strain energy, and dissipation energy are minimal, and the energy curve exhibits a concave upward shape. As loading progresses, the specimens undergo elastic deformation, with input energy primarily converting into elastic strain energy, which increases at an accelerated rate, while dissipation energy remains relatively stable. As the specimens approach peak stress, new cracks form internally, leading to an increase in dissipation energy. During the post-peak stage, microcracks within the specimens continue to expand and coalesce into macroscopic cracks, resulting in a rapid decrease in elastic strain energy and a rapid increase in dissipation energy. This indicates that the specimens experience the most severe damage during this stage.

The YZ projection illustrates the energy change law at peak time. Fig. 10(a) shows that as the hollow diameter increases, the input energy and elastic strain energy of the hollow specimens at peak time gradually decrease, consistent with the trends in peak stress and elastic modulus. Notably, when the hollow diameter increases from 20 mm to 25 mm, the input energy of the specimens decreases most rapidly. Compared to the R-10 specimen, the input energy of the R-30 specimen is reduced by 58.41%, and the elastic strain energy by 64.18%. Additionally, the dissipation energy first increases, then decreases, and then increases again with the increase in hollow diameter, primarily due to the fracture process of the specimens. The R-15 specimen exhibits the highest dissipation energy at peak time, approximately 10.75×10-2 MJ*m-3 , and the post-peak growth rate of dissipation energy is also greater than that of other specimens. Combined with the final failure mode in Fig. 7(b), it is evident that the relative dislocation of rock particles in the R-15 specimen, under internal shear stress, forms a shear fracture zone, resulting in significant internal friction and microcracks. During the compression process, a significant amount of rock debris is ejected, and this kinetic energy further increases the dissipation energy.

The variation trends of input energy and elastic strain energy in rock-backfill specimens are consistent with those in hollow specimens. However, due to tailings backfilling, the fracture complexity of the specimens increases, resulting in a contrasting trend in dissipation energy compared to hollow specimens. At peak time, the dissipation energy of RB-25 and RB-30 specimens is 2.4 times and 2.09 times that of R-25 and R-30 specimens, respectively. This increase is attributed to the heightened fracture degree of the specimens under high stress following tailings backfilling. Additionally, the backfill has low strength and elastic modulus. With larger backfill diameters,

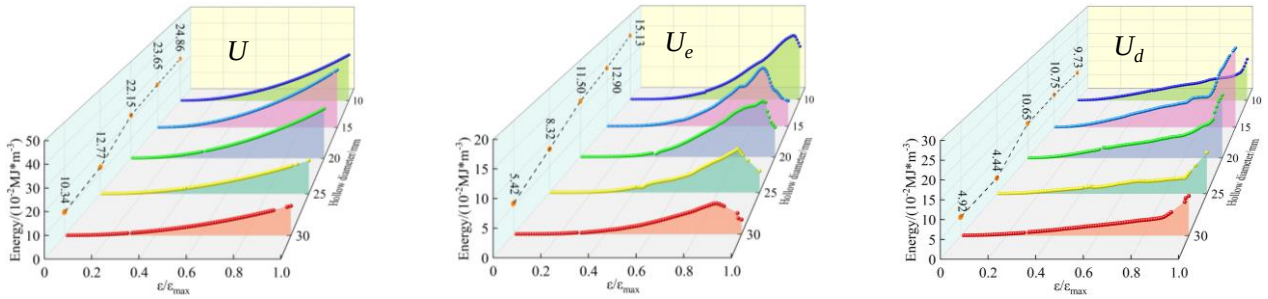

(a) Hollow specimens

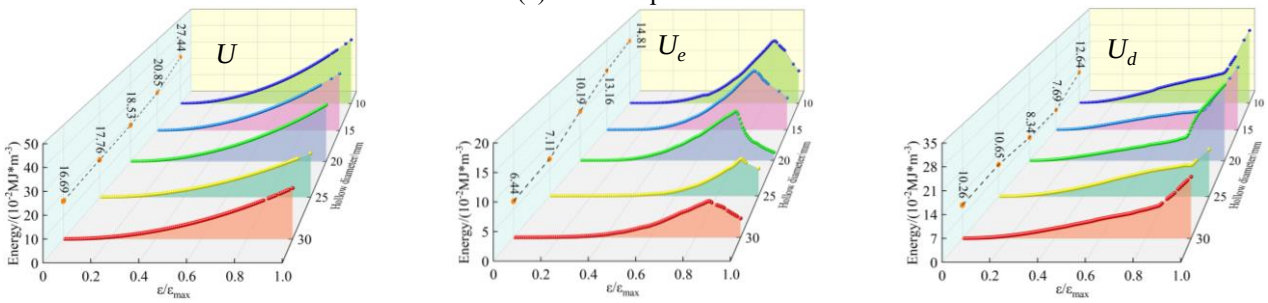

(b) Rock-backfill specimens

Fig. 10 The evolution of U, U_e and U_d of hollow specimens and rock-backfill specimens with strain stage

plastic deformation is more likely under the same stress, leading to increased dissipation energy in the specimens.

4. Acoustic emission parameter response characteristics

4.1 Acoustic emission counts and b-value characteristics

AE counts reflect the activity of microcracks in rock, while the AE *b*-value characterizes the scale distribution of these microcracks. Thus, analyzing the fracture process of rock using AE counts and *b*-value provides a comprehensive evaluation of the rock's damage degree. In seismology, the relationship between earthquake frequency and magnitude is described by the following formula (Gutenberg and Richter 1955)

$$\lg N = a - bM \tag{4}$$

Where: N represents the number of earthquakes, a is a constant, b is the AE *b*-value, and M denotes the earthquake magnitude.

During rock uniaxial compression, the magnitude M can be substituted with amplitude for calculating the AE *b*-value (Zitto *et al*. 2015)

$$\lg N = a - b\left(A_{dB}/20\right) \tag{5}$$

Where: A_{dB} represents the maximum amplitude of AE events.

An increase in the b-value typically indicates the presence of small-scale microfractures. Conversely, a decrease in the *b*-value is usually associated with the formation of large-scale cracks or a significant increase in crack propagation speed. A constant *b*-value suggests a balance in the distribution of both large and small-scale microfractures within the rock. Similar scales of defects produce comparable responses in rocks, leading to consistent variation patterns in AE parameters. Therefore, this study focuses on analyzing the AE parameter characteristics of hollow specimens and rock-backfill specimens with diameters of 10 mm, 20 mm, and 30 mm.

Fig. 11 illustrates the distribution characteristics of AE counts and *b*-values for the specimens. As shown in Fig. 11(a), the AE *b*-value appears after the AE counts, indicating that micropores are gradually closing during this stage, with no new cracks being formed. As loading progresses, crack propagation within the specimens accelerates significantly, leading to a general downward trend in the AE *b*-value. Tailings backfilling inhibits crack formation and propagation to some extent, resulting in a smaller reduction in the *b*-value for the RB-10 specimen compared to the R-10 specimen. Prior to destabilization, the AE *b*-value fluctuates within a narrow range, indicating a steady and progressive failure of the specimens.

Differences are observed in AE counts and *b*-value characteristics between specimens with diameters of 20 mm and 30 mm. As shown in Figs. 11(b) and 11(c), the AE *b*-value for the R-20 and R-30 specimens exhibits an upward trend, in contrast to the R-10 specimen. This indicates that, with increasing hollow diameter, the specimen initially experiences small-scale microfractures. Subsequently, the AE *b*-value for the R-20 specimen dropped sharply, accompanied by a notable increase in AE counts, indicating the formation of large-scale cracks occurring prior to stress fluctuations. The AE *b*-value for the R-30 specimen fluctuates within a narrow range and exhibits an upward trend, indicating stable microcrack propagation and a gradual decrease in crack size. The RB-30 specimen shows progressive stable failure as it approaches the peak, with a

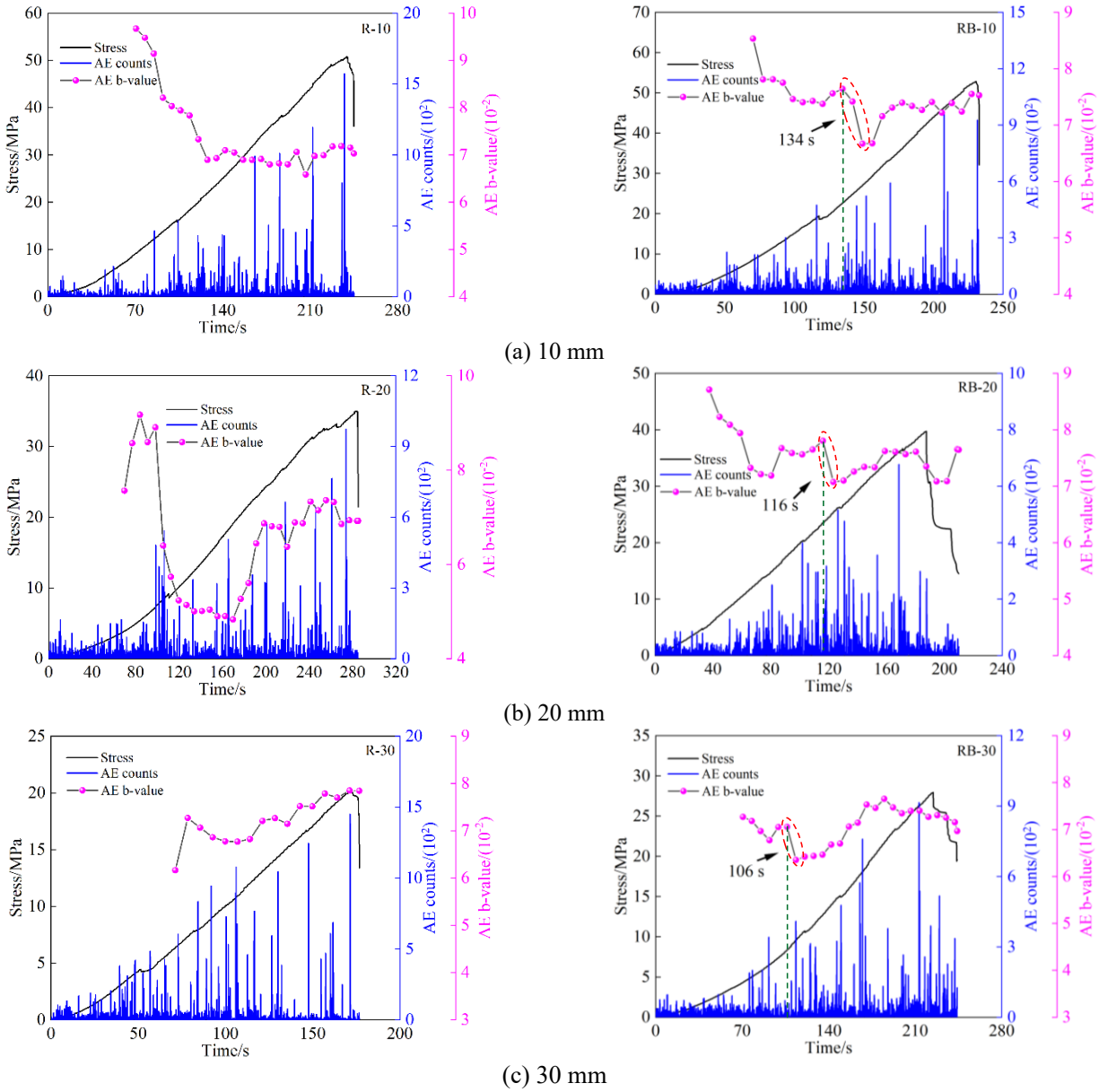

(a) 10 mm

(b) 20 mm

(c) 30 mm

Fig. 11 AE counts and *b*-value Characteristics of hollow specimens and rock-backfill specimens

gradual increase in crack scale. Notably, the AE *b*-value of the RB specimens exhibits a secondary reduction, highlighted by the red dotted line. This phenomenon may result from frictional slip between the tailings backfill and the rock interface. Additionally, a larger backfill diameter corresponds to an earlier occurrence of this phenomenon.

4.2 Acoustic emission AF-RA characteristics

Acoustic emission parameters RA and AF can provide insights into the types of cracks occurring during rock failure (Sun *et al*. 2023). Generally, low RA values combined with high AF values are indicative of tensile cracks, whereas high RA values with low AF values suggest shear cracks. RA represents the ratio of rise time to amplitude, measured in ms/V, while AF denotes the ratio of AE counts to duration, expressed in kHz (Friedrich *et al*. 2021). To differentiate between tensile and shear cracks, this study uses the distinguishing slope k, defined as the

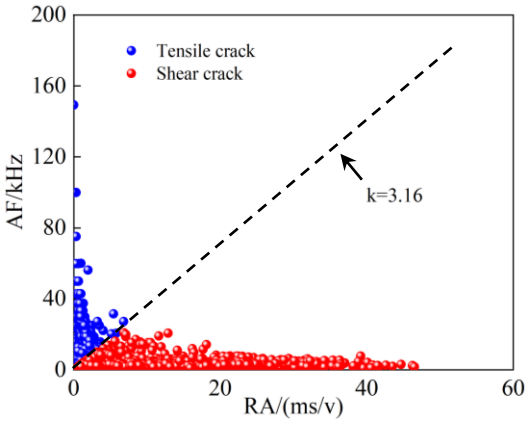

Fig. 12 Rock crack classification and distinguishing slope k

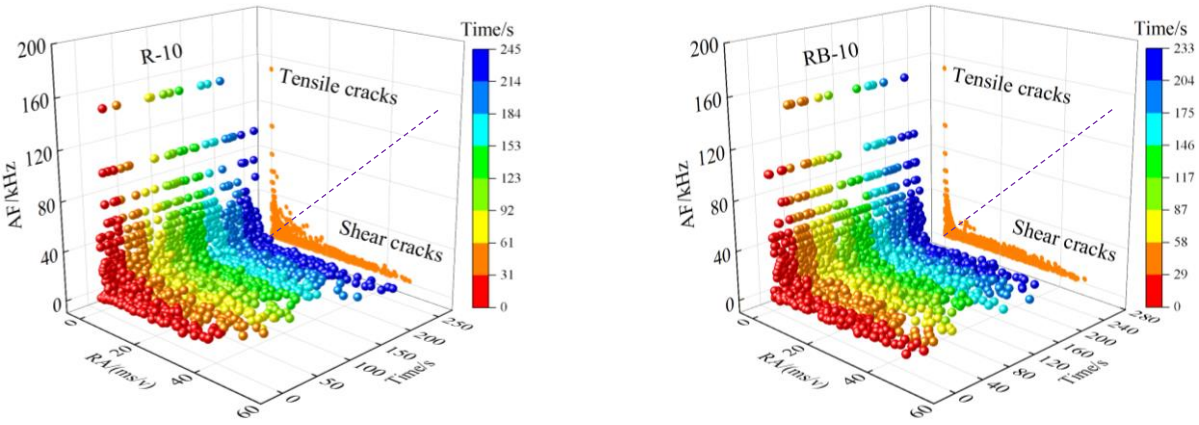

(a) 10 mm

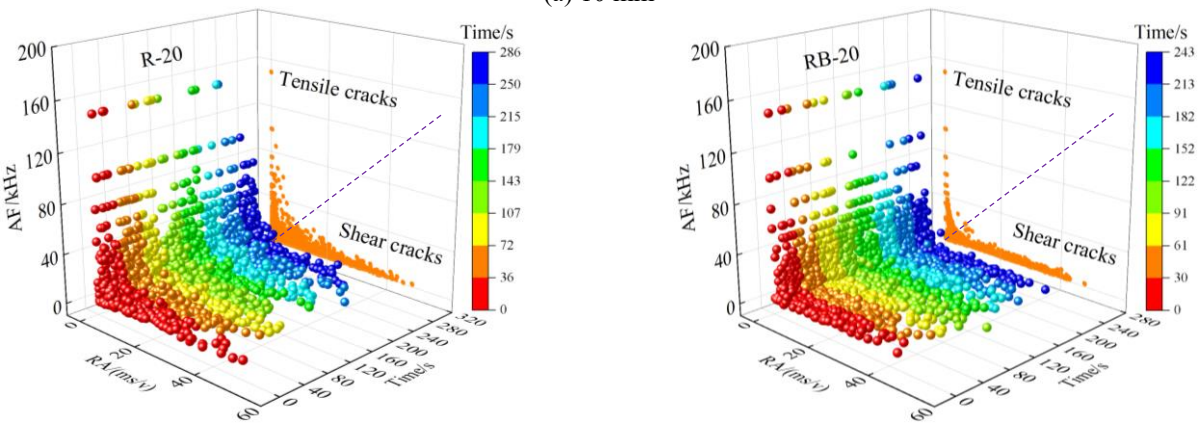

(b) 20 mm

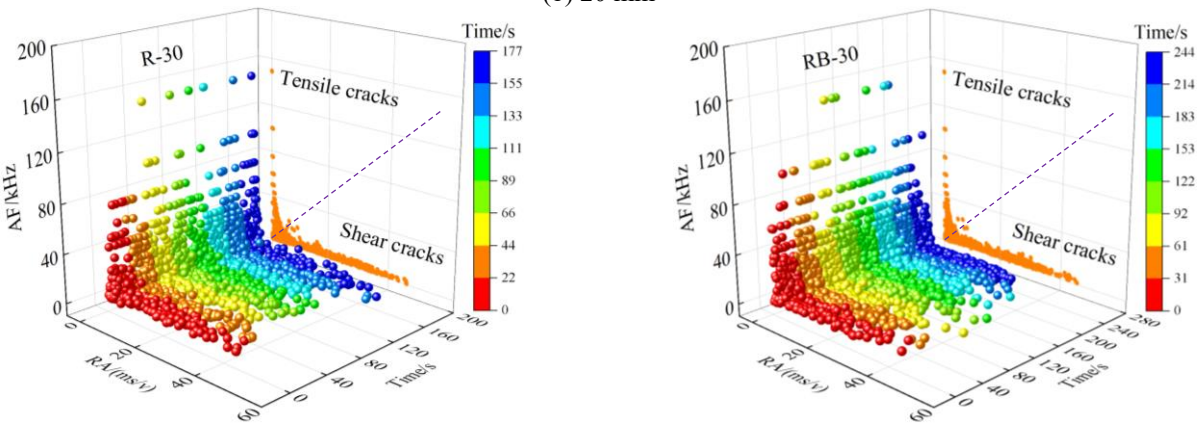

(c) 30 mm

Fig. 13 AE counts and *b*-value Characteristics of hollow specimens and rock-backfill specimens

ratio of AFmax / RAmax (Prem and Murthy 2017), as illustrated in Fig. 12.

Fig. 13 illustrates the distribution of AF and RA signals of specimens at various loading stages. As shown in the figure, AF and RA signals are generated throughout the entire loading process. The data points of the specimens are broadly distributed along the AF axis, ranging from 0 to 160 kHz, with a primary concentration between 0 and 40 kHz. The RA axis is concentrated between 0 and 40 ms/V and is more densely populated, indicating that the failure mode of the specimens is a tensile-shear mixed failure, predominantly involving shear cracks.

The distribution of data points on the AF and RA axes varies slightly among different specimens. Fig. 13(a) shows that RA increases and AF decreases for the R-10 specimen between 220 s and 250 s, indicating a relatively obvious shear failure at this stage. The RA and AF of the RB-10 specimen decrease between 120 s and 160 s. The RA of the R-20 specimen exhibits fluctuating changes, with a higher fluctuation range compared to the RB-20 specimen. This indicates that the R-20 specimen experienced more severe stress release and accumulation during the loading process, with more frequent crack propagation and coalescence. Additionally, the YZ mapping in Fig. 13(b) reveals that the R-20 specimen has the highest density of data points, indicating the largest number of microcracks. Fig. 13(c)

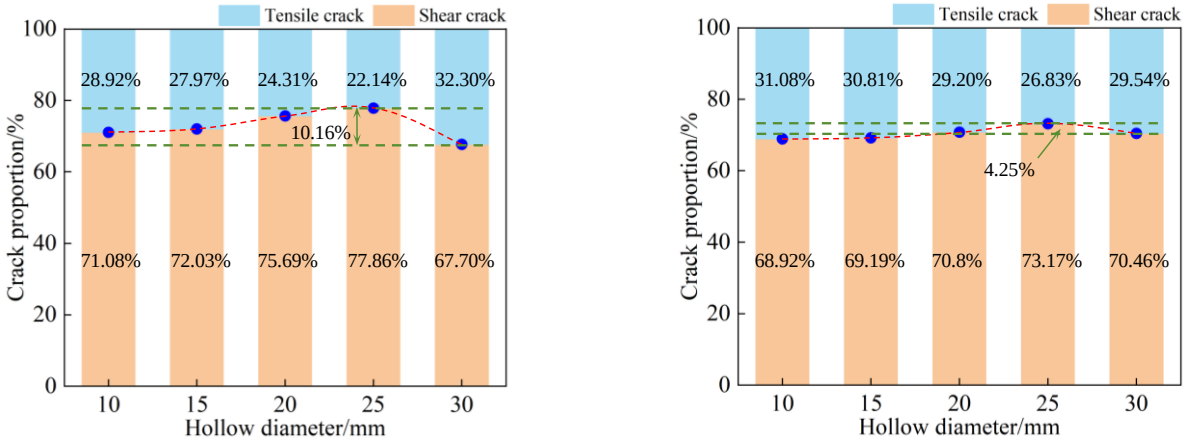

(a) Hollow specimens (b) Rock-backfill specimens

Fig. 14 Proportion of different types of cracks in hollow specimens and rock-backfill specimens

shows that the AF values of the R-30 and RB-30 specimens significantly decrease at the initial stage of loading, with scattered data points of the RB-30 specimen near RA = 40 ms/V.

Fig. 14 illustrates the proportion of tensile and shear cracks in the final failure of the specimens. The figure indicates that shear cracks in hollow and rock-backfill specimens account for approximately 70%, suggesting that the specimens primarily experience tensile-shear mixed failure, with shear cracks playing a dominant role in the failure process. This finding is consistent with the final failure mode of the specimens, indicating a strong correlation between the crack proportions obtained from RA-AF signal analysis and the actual cracks. As the hollow diameter increases, the proportion of shear cracks first increases and then decreases. The proportion of shear cracks is highest in the R-25 specimen, at approximately 77.86%, whereas the R-30 specimen has the highest proportion of tensile cracks, at about 32.30%, as depicted in Fig. 14(a). The trend in the proportion of shear cracks in rock-backfill specimens mirrors that of hollow specimens, though the variation is more gradual, as shown in Fig. 14(b).

5. Conclusions

To investigate the stability of tailings backfill goaf with varying structural properties, uniaxial compression tests were conducted on hollow and rock-backfill specimens, and their mechanical parameter characteristics were analyzed. The fracture behavior of the specimens was examined basedon acoustic emission characteristics and energy evolution. The main conclusions are summarized as follows:

- As the hollow diameter increases, the peak strength and elastic modulus of the hollow specimens gradually decrease, and the strain corresponding to the stress fluctuation point also decreases. Compared to the complete specimen, the peak strength and elastic modulus of the R-30 specimen decrease by 65.77% and 65.99%, respectively. Tailings backfilling enhances the peak strength and elastic modulus of the specimens, but does not alter their overall trend.
- As the hollow diameter increases, the crack network phenomenon on the surface of the hollow specimens gradually diminishes. The rock debris transition from small spalled and ejected pieces to larger spalled fragments. The crack propagation pattern of the rock-backfill specimens is similar, exhibiting a V-shaped distribution. The final failure mode of the specimens is a tensile-shear mixed failure, predominantly shear failure. The internal backfill predominantly exhibits shear slip failure.
- The input energy U and elastic strain energy U_e at the peak time are positively correlated with the variation of mechanical parameters. The dissipation energy U_d is related to the fracture process of the specimens. The dissipation energy of the hollow specimens initially increases, then decreases, and subsequently increases. The variation trend of dissipation energy in rock-backfill specimens is opposite to that of hollow specimens. The dissipation energy of the RB-25 specimen is approximately 2.4 times that of the R-25 specimen.
- The AE b-value of the rock-backfill specimens shows a secondary decrease phenomenon. With the increase in backfill diameter, this phenomenon appears earlier. The fluctuation of the RA value is significant, suggesting more severe stress release and crack propagation coalescence behavior, with a larger number of microcracks. With the increase in diameter, the proportion of shear cracks in the specimens initially increases and then decreases, but the change in rock-backfill specimens is more gradual.

In summary, the findings of this study are of great significance for optimizing stope structures and improving the stability of deep mining stopes. However, the impact of the microstructural characteristics of tailings backfill on its fracture mechanism remains unclear. In future work, numerical simulations, nuclear magnetic resonance (NMR), and CT scanning will be employed to further investigate the microscopic fracture mechanisms.

Acknowledgments

The research was financially supported by the National Natural Science Foundation of China (No. 52204137), and the Outstanding Young Scientific and Technological Talents Project of Liaoning University of Science and Technology (No. 2023YQ10), and the Education Department Foundation of Liaoning Province (No. LJKQZ20222317). The Postdoctoral Fellowship Program of CPSF (No. GZC20231479). The China Postdoctoral Science Foundation (2024M751813)

References

Aubertin, M., Li, L., Arnoldi, S., Belem, T., Bussière, B., Benzaazoua, M. and Simon, R. (2003), "Interaction between backfill and rock mass in narrow stopes", *Soil Rock Am.*, **1**(2), 1157-1164.

Chiloane, N.M., Sengani, F. and Mulenga, F. (2024), "An experimental and numerical study of the strength development of layered cemented tailings backfill", *Sci. Rep-Uk.*, **14**(1), 734. https://doi.org/10.1038/s41598-024-51464-2.

Choudhary, B.S. and Kumar, S. (2013), "Underground void filling by cemented mill tailings", *Int. J. Min. Sci. Technol.*, **23**(6), 893-900. https://doi.org/10.1016/j.ijmst.2013.11.003.

Fall, M., Benzaazoua, M. and Ouellet, S. (2005), "Experimental characterization of the influence of tailings fineness and density on the quality of cemented paste backfill", *Miner. Eng.*, **18**(1), 41-44. https://doi.org/10.1016/j.mineng.2004.05.012.

Fall, M., Célestin, J.C., Pokharel, M. and Toure, M. (2010), "A contribution to understanding the effects of curing temperature on the mechanical properties of mine cemented tailings backfill", *Eng. Geol.*, **114**(3-4), 397-413. https://doi.org/10.1016/j.enggeo.2010.05.016.

Friedrich, L., Colpo, A., Maggi, A., Becker, T., Lacidogna, G. and Iturrioz, I. (2021), "Damage process in glass fiber reinforced polymer specimens using acoustic emission technique with low frequency acquisition", *Compos. Struct.*, **256**, 113105. https://doi.org/10.1016/j.compstruct.2020.113105.

Fu J.X., Wang J. and Song W.D. (2020), "Damage constitutive model and strength criterion of cemented paste backfill based on layered effect considerations", *J. Mater. Res. Technol.*, **9**(3), 6073-6084. https://doi.org/10.1016/j.jmrt.2020.04.011.

Golik, V.I., and Efremenkov, A.B. (2017), "Control of rock mechanics in underground ore mining", *IOP Conference Series: Materials Science and Engineering. IOP Publishing*, **221**(1), 012013. https://doi.org/10.1088/1757-899X/221/1/012013.

Gutenberg, B. and Richter, C.F. (1955), "Magnitude and energy of earthquakes", *Nature*, **176**(4486), 795-795.

Hane, I., Belem, T., Benzaazoua, M. and Maqsoud, A. (2017), "Laboratory characterization of cemented tailings paste containing crushed waste rocks for improved compressive strength development", *Geotech. Geol. Eng.*, **35**, 645-662. https://doi.org/10.1007/s10706-016-0131-6.

Helinski, M., Fahey, M. and Fourie, A. (2010), "Coupled two-dimensional finite element modelling of mine backfilling with cemented tailings", *Can. Geotech. J.*, **47**(11), 1187-1200. https://doi.org/10.1139/t10-020.

Hou, Y.Q., Yin, S.H., Chen, X., Zhang, M.Z. and Yang, S.X. (2021), "Study on characteristic stress and energy damage evolution mechanism of cemented tailings backfill under uniaxial compression", *Constr. Build. Mater.*, **301**, 124333. https://doi.org/10.1016/j.conbuildmat.2021.124333.

Kasap, T., Yilmaz, E. and Sari, M. (2022), "Physico-chemical and micro-structural behavior of cemented mine backfill: Effect of pH in dam tailings", *J. Environ. Manage.*, **314**, 115034. https://doi.org/10.1016/j.jenvman.2022.115034.

Kesimal, A., Yilmaz, E. and Ercikdi, B. (2004), "Evaluation of paste backfill mixtures consisting of sulphide-rich mill tailings and varying cement contents", *Cement Concrete Res.*, **34**(10), 1817-1822. https://doi.org/10.1016/j.cemconres.2004.01.018.

Kim, E., Garcia, A. and Changani, H. (2018), "Fragmentation and energy absorption characteristics of Red, Berea and Buff sandstones based on different loading rates and water contents", *Geomech. Eng.*, **14**(2), 151-159. https://doi.org/10.12989/gae.2018.14.2.151.

Kongar-Syuryun, Ch., Aleksakhin, A., Khayrutdinov, A. and Tyulyaeva, Y. (2021), "Research of rheological characteristics of the mixture as a way to create a new backfill material with specified characteristics", *Materials Today: Proceedings*, **38**, 2052-2054. https://doi.org/10.1016/j.matpr.2020.10.139.

Komurlu, E., Kesimal, A. and Demir, S. (2016), "Experimental and numerical analyses on determination of indirect (splitting) tensile strength of cemented paste backfill materials under different loading apparatus", *Geomech. Eng.*, **10**(6), 775-791. https://doi.org/10.12989/gae.2016.10.6.775.

Kumar, D., Singh, U.K. and Singh, G.S.P. (2016), "Laboratory characterization of cemented rock fill for underhand cut and fill method of mining", *J. Institution of Engineers (India): Series D*, **97**, 193-203. https://doi.org/10.1007/s40033-015-0088-2.

Li, J.J., Cao, S. and Yilmaz, E. (2021), "Characterization of macro mechanical properties and microstructures of cement-based composites prepared from fly ash, gypsum and steel slag", *Minerals-Basel.*, **12**(1), 6. https://doi.org/10.3390/min12010006.

Ma Q., Liu X.L., Tan Y.L., Wang, R.S., Xie, W.Q., Wang, E.Z., Liu, X.S. and Shang, J.L. (2024), "Experimental study of loading system stiffness effects on mechanical characteristics and kinetic energy calculation of coal specimens", *Rock Mech. Rock Eng.*, 1-17. https://doi.org/10.1007/s00603-024-04054-7.

Ozcan, N.T., Ulusay, R. and Isik, N.S. (2013), "A study on geotechnical characterization and stability of downstream slope of a tailings dam to improve its storage capacity (Turkey)", *Environ. Earth Sci.*, **69**, 1871-1890. https://doi.org/10.1007/s12665-012-2016-1.

Palchik, V. (2002), "Influence of physical characteristics of weak rock mass on height of caved zone over abandoned subsurface coal mines", *Environ. Geol.*, **42**(1), 92-101. https://doi.org/10.1007/s00254-002-0542-y.

Prem, P.R. and Murthy, A.R. (2017), "Acoustic emission monitoring of reinforced concrete beams subjected to four-point-bending", *Appl. Acoust.*, **117**, 28-38. https://doi.org/10.1016/j.apacoust.2016.08.006.

Sari M., Yilmaz E., Kasap T. and Guner, N.U. (2022), "Strength and microstructure evolution in cemented mine backfill with low and high pH pyritic tailings: Effect of mineral admixtures", *Constr. Build. Mater.*, **328**, 127109. https://doi.org/10.1016/j.conbuildmat.2022.127109.

Sharafisafa, M., Shen, L., Zheng, Y. and Xiao, J. (2019), "The effect of flaw filling material on the compressive behaviour of 3D printed rock-like discs", *Int. J. Rock. Mech. Min.*, **117**, 105-117. https://doi.org/10.1016/j.ijrmms.2019.03.031.

Shiotani, T. (2006), "Evaluation of long-term stability for rock slope by means of acoustic emission technique", *Ndt & E Int.*, **39**(3), 217-228. https://doi.org/10.1016/j.ndteint.2005.07.005.

Siddique, S. and Jang, J.G. (2020), "Assessment of molybdenum mine tailings as filler in cement mortar", *J. Build. Eng.*, **31**, 101322. https://doi.org/10.1016/j.jobe.2020.101322.

Song, X.P., Li, J.B., Wang, S., Zhou, S., Liu, W., Zhai, Y.K. and Hao, Y.X. (2022), "Study of mechanical behavior and cracking mechanism of prefabricated fracture cemented paste backfill under different loading rates from the perspective of energy

evolution", *Constr. Build. Mater.*, **361**, 129737. https://doi.org/10.1016/j.conbuildmat.2022.129737.

Song, X.P., Yu, X., Zhao, W.H., Yang, F.G., Shi, J.Y. and Yalçınkaya, Ç. (2023), "Progressive damage process and destabilization precursor recognition of sulfate tailing-cemented paste backfill based on acoustic emission", *Powder Technol.*, **430**, 119047. https://doi.org/10.1016/j.powtec.2023.119047.

Sun, B., Yang, H.W., Zeng, S., Yin, Y. and Fan, J.W. (2023), "Crack initiation mechanism and meso-crack evolution of pre-fabricated cracked sandstone specimens under uniaxial loading", *Geomech. Eng.*, **33**(6), 597-609. https://doi.org/10.12989/gae.2023.33.6.597.

Tan, Y.Y., Zhang, K., Yu, X., Song, W.D., Wang, J. and Hai, C.L. (2020), "The mechanical and microstructural properties of composite structures made of a cement-tailing backfill and rock core", *Minerals-Basel.*, **10**(2), 159. https://doi.org/10.3390/min10020159.

Ullah, B., Zhou, Z., Cai, X., Lu, J. and Zhao, C.C. (2023), "Failure prediction and microcracks development based on acoustic emission and energy evolution for different rocks treated with freeze–thaw weathering", *B. Eng. Geol. Environ.*, **82**(12), 471. https://doi.org/10.1007/s10064-023-03485-w.

Xue, G.L., Yilmaz, E., Feng, G.R. and Cao, S. (2021), "Bending behavior and failure mode of cemented tailings backfill composites incorporating different fibers for sustainable construction", *Constr. Build. Mater.*, **289**, 123163. https://doi.org/10.1016/j.conbuildmat.2021.123163.

Yan, B.X., Jia, H.W., Yilmaz, E., Lai, X.P., Shan, P.F. and Hou, C. (2022), "Numerical study on microscale and macroscale strength behaviors of hardening cemented paste backfill", *Constr. Build. Mater.*, **321**, 126327. https://doi.org/10.1016/j.conbuildmat.2022.126327.

Yilmaz, E. (2011), "Advances in reducing large volumes of environmentally harmful mine waste rocks and tailings", *Gospod. Surowcami Min.*, 89-112.

Yilmaz, E., Belem, T., Benzaazoua, M. and Bussière, B. (2010), "Assessment of the modified CUAPS apparatus to estimate in situ properties of cemented paste backfill", *Geotech. Test. J.*, **33**(5), 351-362. https://doi.org/10.1520/GTJ102689.

Zhou, Y., Yin, S.H., Zhao, K., Wang, L.M. and Liu, L. (2023), "Understanding the static rate dependence of early fracture behavior of cemented paste backfill using digital image correlation and acoustic emission techniques", *Eng. Fract. Mech.*, **283**, 109209. https://doi.org/10.1016/j.engfracmech.2023.109209.

Zitto, M.E., Piotrkowski, R., Gallego, A., Sagasta, F. and Benavent-Climent, A. (2015), "Damage assessed by wavelet scale bands and b-value in dynamical tests of a reinforced concrete slab monitored with acoustic emission", *Mech. Syst. Signal Pr.*, **60**, 75-89. https://doi.org/10.1016/j.ymssp.2015.02.006.